J|A|C|S
ARTICLES
Published on Web 02/12/2005

A New Spin Probe of Protein Dynamics: Nitrogen Relaxation in $^{15}N-^{2}H$ Amide Groups

Jun Xu,[†] Oscar Millet,[‡] Lewis E. Kay,[‡] and Nikolai R. Skrynnikov*,[†]

Contribution from the Department of Chemistry, Purdue University, West Lafayette, Indiana 47907, and Departments of Medical Genetics, Biochemistry, and Chemistry, University of Toronto, Toronto, Ontario M5S 1A8, Canada

Received September 13, 2004; E-mail: nikolai@purdue.edu

Abstract: ^{15}N spin relaxation data have provided a wealth of information on protein dynamics in solution. Standard R_1, $R_{1\rho}$, and NOE experiments aimed at $^{15}N[^{1}H]$ amide moieties are complemented in this work by HA(CACO)N-type experiments allowing the measurement of nitrogen R_1 and $R_{1\rho}$ rates at deuterated $^{15}N[^{2}D]$ sites. Difference rates obtained using this approach, $R_1(^{15}N[^{1}H]) - R_1(^{15}N[^{2}D])$ and $R_2(^{15}N[^{1}H]) - R_2(^{15}N[^{2}D])$, depend exclusively on dipolar interactions and are insensitive to ^{15}N CSA and R_{ex} relaxation mechanisms. The methodology has been tested on a sample of peptostreptococcal protein L (63 residues) prepared in 50% $H_2O-50\%$ D_2O solvent. The results from the new and conventional experiments are found to be consistent, with respect to both local backbone dynamics and overall protein tumbling. Combining several data sets permits evaluation of the spectral density $J(\omega_D + \omega_N)$ for each amide site. This spectral density samples a uniquely low frequency (26 MHz at a 500 MHz field) and, therefore, is expected to be highly useful for characterizing nanosecond time scale local motions. The spectral density mapping demonstrates that, in the case of protein L, $J(\omega_D + \omega_N)$ values are compatible with the Lipari−Szabo interpretation of backbone dynamics based on the conventional ^{15}N relaxation data.

Introduction

Since their inception at the end of the 1980s,[1] ^{15}N R_1, R_2, and $^{1}H-^{15}N$ heteronuclear NOE experiments have been the primary source of information on the mobility of proteins in solution. These HSQC-based experiments do not require any special isotope labeling beyond the standard ^{15}N enrichment and are highly sensitive, simple to set up, and, in general, straightforward to interpret. ^{15}N spin relaxation studies in the past have been used to delineate the relationship between fast dynamics and protein−protein interactions,[2−5] protein−nucleic acid interactions,[6−10] ligand binding,[11−16] enzyme catalysis,[17,18] protein aggregation[19−21] and stability,[22] properties of folding intermediates,[23−25] and properties of unfolded proteins.[26−29] In addition, the relative orientation of domains in multidomain proteins[30−32] and domain motions[33,34] have also been investigated using ^{15}N relaxation data.

[†] Purdue University.
[‡] University of Toronto.

(1) Kay, L. E.; Torchia, D. A.; Bax, A. *Biochemistry* **1989**, *28*, 8972−8979.
(2) Kay, L. E.; Muhandiram, D. R.; Wolf, G.; Shoelson, S. E.; Forman-Kay, J. D. *Nat. Struct. Biol.* **1998**, *5*, 156−163.
(3) Carr, P. A.; Erickson, H. P.; Palmer, A. G. *Structure* **1997**, *5*, 949−959.
(4) Oz, G.; Zangger, K.; Armitage, I. M. *Biochemistry* **2001**, *40*, 11433−11441.
(5) Wang, C. Y.; Pawley, N. H.; Nicholson, L. K. *J. Mol. Biol.* **2001**, *313*, 873−887.
(6) Bracken, C.; Carr, P. A.; Cavanagh, J.; Palmer, A. G. *J. Mol. Biol.* **1999**, *285*, 2133−2146.
(7) Markus, M. A.; Hinck, A. P.; Huang, S. R.; Draper, D. E.; Torchia, D. A. *Nat. Struct. Biol.* **1997**, *4*, 70−77.
(8) Yu, L. P.; Zhu, C. X.; Tse-Dinh, Y. C.; Fesik, S. W. *Biochemistry* **1996**, *35*, 9661−9666.
(9) Maciejewski, M. W.; Liu, D. J.; Prasad, R.; Wilson, S. H.; Mullen, G. P. *J. Mol. Biol.* **2000**, *296*, 229−253.
(10) Feng, W. Q.; Tejero, R.; Zimmerman, D. E.; Inouye, M.; Montelione, G. T. *Biochemistry* **1998**, *37*, 10881−10896.
(11) Gagné, S. M.; Tsuda, S.; Spyracopoulos, L.; Kay, L. E.; Sykes, B. D. *J. Mol. Biol.* **1998**, *278*, 667−686.
(12) Hodsdon, M. E.; Cistola, D. P. *Biochemistry* **1997**, *36*, 2278−2290.
(13) Constantine, K. L.; Friedrichs, M. S.; Wittekind, M.; Jamil, H.; Chu, C. H.; Parker, R. A.; Goldfarb, V.; Mueller, L.; Farmer, B. T. *Biochemistry* **1998**, *37*, 7965−7980.
(14) Stivers, J. T.; Abeygunawardana, C.; Mildvan, A. S.; Whitman, C. P. *Biochemistry* **1996**, *35*, 16036−16047.
(15) Garcia, F. L.; Szyperski, T.; Dyer, J. H.; Choinowski, T.; Seedorf, U.; Hauser, H.; Wüthrich, K. *J. Mol. Biol.* **2000**, *295*, 595−603.
(16) Zidek, L.; Novotny, M. V.; Stone, M. J. *Nat. Struct. Biol.* **1999**, *6*, 1118−1121.
(17) Osborne, M. J.; Schnell, J.; Benkovic, S. J.; Dyson, H. J.; Wright, P. E. *Biochemistry* **2001**, *40*, 9846−9859.
(18) Freedberg, D. I.; Ishima, R.; Jacob, J.; Wang, Y. X.; Kustanovich, I.; Louis, J. M.; Torchia, D. A. *Protein Sci.* **2002**, *11*, 221−232.
(19) Fushman, D.; Cahill, S.; Cowburn, D. *J. Mol. Biol.* **1997**, *266*, 173−194.
(20) Viles, J. H.; Donne, D.; Kroon, G.; Prusiner, S. B.; Cohen, F. E.; Dyson, H. J.; Wright, P. E. *Biochemistry* **2001**, *40*, 2743−2753.
(21) Bocharov, E. V.; Korzhnev, D. M.; Blommers, M. J. J.; Arvinte, T.; Orekhov, V. Y.; Billeter, M.; Arseniev, A. S. *J. Biol. Chem.* **2002**, *277*, 46273−46279.
(22) Beeser, S. A.; Goldenberg, D. P.; Oas, T. G. *J. Mol. Biol.* **1997**, *269*, 154−164.
(23) Eliezer, D.; Chung, J.; Dyson, H. J.; Wright, P. E. *Biochemistry* **2000**, *39*, 2894−2901.
(24) Kortemme, T.; Kelly, M. J. S.; Kay, L. E.; Forman-Kay, J.; Serrano, L. *J. Mol. Biol.* **2000**, *297*, 1217−1229.
(25) Yao, J.; Chung, J.; Eliezer, D.; Wright, P. E.; Dyson, H. J. *Biochemistry* **2001**, *40*, 3561−3571.
(26) Farrow, N. A.; Zhang, O. W.; Forman-Kay, J. D.; Kay, L. E. *Biochemistry* **1997**, *36*, 2390−2402.
(27) Cho, H. S.; Liu, C. W.; Damberger, F. F.; Pelton, J. G.; Nelson, H. C. M.; Wemmer, D. E. *Protein Sci.* **1996**, *5*, 262−269.
(28) Schwalbe, H.; Fiebig, K. M.; Buck, M.; Jones, J. A.; Grimshaw, S. B.; Spencer, A.; Glaser, S. J.; Smith, L. J.; Dobson, C. M. *Biochemistry* **1997**, *36*, 8977−8991.
(29) Sinclair, J. F.; Shortle, D. *Protein Sci.* **1999**, *8*, 991−1000.
(30) Brüschweiler, R.; Liao, X. B.; Wright, P. E. *Science* **1995**, *268*, 886−889.
(31) Fushman, D.; Xu, R.; Cowburn, D. *Biochemistry* **1999**, *38*, 10225−10230.
(32) Hwang, P. M.; Skrynnikov, N. R.; Kay, L. E. *J. Biomol. NMR* **2001**, 20, 83−88.

10.1021/ja040215z CCC: $30.25

Despite the strengths of nitrogen relaxation studies, there are certain complexities and limitations that must be considered. For example, the exact values of the nitrogen chemical shift anisotropy $\Delta\sigma_N$[35,36] and the proton−nitrogen bond length r_{NH},[37] as well as the site variability of these two parameters, have been the subject of discussion. In addition, R_2 data often contain small contributions that may be attributed to microsecond−millisecond chemical exchange. The reliable identification of exchange terms requires additional studies.[38,39] Furthermore, a number of minor relaxation contributions, such as dipolar relaxation from covalently bonded carbon nuclei, proximal protons, and solvent,[40] as well as relaxation due to the antisymmetric component of nitrogen CSA,[41,42] can each contribute 1−2% to the measured rate. Inclusion of these minor terms in the interpretation procedure can be tedious and complicated. Finally, ^{15}N relaxation data do not always provide a good sampling of fast local motions. For instance, they are insensitive to roll-type motion of α-helices.[43]

Given the significance of ^{15}N spin relaxation studies and the limitations described above, it is important to develop alternative experiments to validate the standard approach. With this in mind, we introduce a new relaxation probe—namely, the ^{15}N spin which is part of a $^{15}N-^{2}D$ backbone amide group. The substitution of a deuteron for a proton involves a minimum perturbation to the structure and dynamics of the peptide plane. The measurement of $^{15}N[^{2}D]$ relaxation rates provides information that is complementary to conventional data. Notably, these rates are dependent on the spectral density term $J(\omega_D + \omega_N)$, which, due to the opposite signs of ω_D and ω_N, samples a very low frequency ($(\omega_D + \omega_N)/2\pi = 26$ MHz at a 500 MHz field). It therefore becomes possible to better define the spectral density profile, especially with regard to local dynamics that occur on the intermediate time scale, ∼1 ns.

It is clear that amide protons cannot be used as either the source of magnetization or as the point of detection in $^{15}N[^{2}D]$ relaxation experiments. Instead, the HA(CACO)N sequence[44,45] that begins and ends with H^{α} magnetization was adapted for these measurements. The new methodology has been tested on the 63-residue B1 immunoglobulin-binding domain of protein L.[46] We demonstrate that the results are broadly consistent with conventional ^{15}N relaxation experiments and that the new data can be used to estimate the rotational diffusion parameters of the protein to good accuracy. Finally, we present a spectral density mapping procedure to extract $J(\omega_D + \omega_N)$ and show that the spectral density function is well described by a Lorentzian profile, as expected.

Materials and Methods

Sample. A uniform ^{13}C,^{15}N-labeled sample of protein L was expressed and purified as described elsewhere.[47] The protein was denatured by the application of 3.5 M guanidinium chloride in a solution comprised of 50% H_2O−50% D_2O, and then refolded and lyophilized. The NMR sample was subsequently prepared using (approximately) 50% H_2O−50% D_2O solvent so that $^{15}N-^{1}H$ and $^{15}N-^{2}D$ relaxation measurements could be performed on the same sample. An alternative approach involving two different samples (one with H_2O and the other with D_2O as solvents) would effectively improve the sensitivity of the measurements by $\sqrt{2}$. However, differences in viscosities between the two samples would complicate a comparison of the data. The pH of the sample was adjusted to 5.0 (uncorrected for the isotope effect). H−D exchange rates at pH 5.0 and 25 °C do not exceed 0.1 s^{-1} even for solvent-exposed protons,[48,49] and in what follows we demonstrate that the exchange with solvent does not affect the outcome of our measurements. Sample conditions were 1.8 mM protein, 50 mM phosphate buffer, and 0.05% NaN_3. Relaxation data sets were recorded at 600 and 500 MHz using Varian Inova spectrometers equipped with triple-resonance *z*-axis gradient probes.

NMR Experiments. The HA(CACO)N-based sequence[44,45] used for the measurement of R_1 and $R_{1\rho}$ relaxation rates in $^{15}N[^{1}H/^{2}D]$ moieties is shown in Figure 1. The magnetization transfer scheme can be outlined as follows:

$$H_z^{\alpha}\,(a) \rightarrow H_z^{\alpha}C_z^{\alpha}\,(b) \rightarrow C_z^{\alpha}C_z'\,(c) \rightarrow C_z'N_z\,(d, e) \rightarrow$$
$$C_z'N_z/C_z'N_x\,(\text{relaxation}) \rightarrow C_z'N_x\,(t_1) \rightarrow \ldots \rightarrow H_x^{\alpha}\,(\text{detection}) \quad (1)$$

where the letters in parentheses placed after the spin operators refer to the points highlighted in the pulse sequence of Figure 1. The magnetization transfer from $C_z'N_x$ back to H_x^{α} follows the reverse of the transfer pathway detailed in the scheme of eq 1. In what follows only the elements of the experiment that are distinct from previous HA(CACO)N sequences are described.

Central to the operation of the sequence is the element inserted between points d and e that serves to discriminate between the $^{15}N[^{1}H]$ and $^{15}N[^{2}D]$ moieties. After the ^{15}N 90° pulse following point d in the sequence the magnetization of interest is given by $C_z'N_y$. In the case of the $^{15}N[^{1}H]$ group, subsequent evolution during the period $2\tau_e-180°(^{1}H)-2\tau_e$, where $2\tau_e = 1/(2J_{NH})$ and a 180° proton pulse is applied in alternate scans (dotted outline in Figure 1), encodes this coherence as $\pm C_z'N_y$. By contrast, in the case of the deuterated amide group the coherence of interest $C_z'N_y$ remains unchanged (note that scalar relaxation of the second kind is suppressed by deuterium decoupling).

Spectra with and without the ^{1}H 180° pulse between points d and e are recorded in an interleaved manner. The corresponding spectral traces along the F1(ω_N) dimension are shown in Figure 2a,b for residue Glu-27. The subtraction and addition of time- or frequency-domain data allows for the separation of $^{1}H^{\alpha}-^{15}N[^{1}H]$ and $^{1}H^{\alpha}-^{15}N[^{2}D]$ correlations (illustrated in parts c and d, respectively, of Figure 2). Note that the $^{15}N[^{1}H]$ and $^{15}N[^{2}D]$ signals are separated by an isotopic shift of 0.7 ppm.[50] This can be used to establish the absence of exchange with solvent during the relaxation period, as discussed below.

The selection element, d−e, is followed in the pulse sequence by a relaxation period shown in Figure 1, insets A and B (R_1 and $R_{1\rho}$ experiments, respectively). Note that in what follows we refer to the relaxation experiments using the notations R_1 and $R_{1\rho}$ although, strictly

(33) Lee, B. M.; De Guzman, R. N.; Turner, B. G.; Tjandra, N.; Summers, M. F. *J. Mol. Biol.* **1998**, *279*, 633−649.
(34) Baber, J. L.; Szabo, A.; Tjandra, N. *J. Am. Chem. Soc.* **2001**, *123*, 3953−3959.
(35) Cornilescu, G.; Bax, A. *J. Am. Chem. Soc.* **2000**, *122*, 10143−10154.
(36) Fushman, D.; Cowburn, D. *Methods Enzymol.* **2001**, *339*, 109−126.
(37) Case, D. A. *J. Biomol. NMR* **1999**, *15*, 95−102.
(38) Desvaux, H.; Birlirakis, N.; Wary, C.; Berthault, P. *Mol. Phys.* **1995**, *86*, 1059−1073.
(39) Millet, O.; Loria, J. P.; Kroenke, C. D.; Pons, M.; Palmer, A. G. *J. Am. Chem. Soc.* **2000**, *122*, 2867−2877.
(40) Halle, B. *J. Chem. Phys.* **2003**, *119*, 12372−12385.
(41) Kowalewski, J.; Werbelow, L. *J. Magn. Reson.* **1997**, *128*, 144−148.
(42) Scheurer, C.; Skrynnikov, N. R.; Lienin, S. F.; Straus, S. K.; Brüschweiler, R.; Ernst, R. R. *J. Am. Chem. Soc.* **1999**, *121*, 4242−4251.
(43) Fischer, M. W. F.; Zeng, L.; Majumdar, A.; Zuiderweg, E. R. P. *Proc. Natl. Acad. Sci. U.S.A.* **1998**, *95*, 8016−8019.
(44) Wang, A. C.; Grzesiek, S.; Tschudin, R.; Lodi, P. J.; Bax, A. *J. Biomol. NMR* **1995**, *5*, 376−382.
(45) Kanelis, V.; Donaldson, L.; Muhandiram, D. R.; Rotin, D.; Forman-Kay, J. D.; Kay, L. E. *J. Biomol. NMR* **2000**, *16*, 253−259.
(46) Scalley, M. L.; Yi, Q.; Gu, H. D.; McCormack, A.; Yates, J. R.; Baker, D. *Biochemistry* **1997**, *36*, 3373−3382.
(47) Mittermaier, A.; Kay, L. E. *J. Am. Chem. Soc.* **1999**, *121*, 10608−10613.
(48) Molday, R. S.; Englander, S. W.; Kallen, R. G. *Biochemistry* **1972**, *11*, 150−158.
(49) Englander, S. W.; Englander, J. J. *Methods Enzymol.* **1978**, *49*, 24−39.
(50) Jaravine, V. A.; Cordier, F.; Grzesiek, S. *J. Biomol. NMR* **2004**, *29*, 309−318.

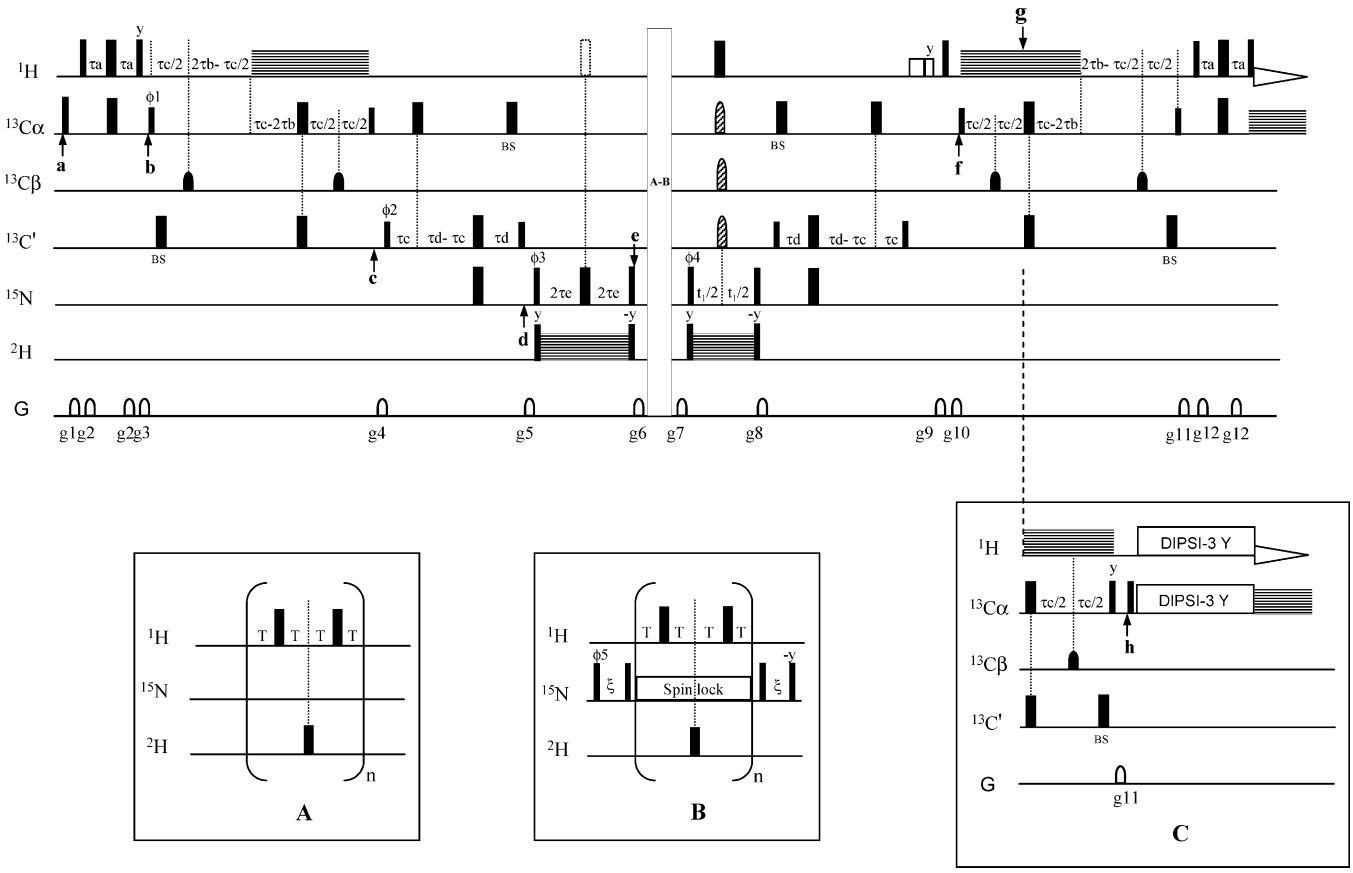

Figure 1. Pulse sequences for measuring longitudinal $R_1(C_z'N_z[^1H/^2D])$ (A) and transverse $R_{1\rho}(C_z'N_x[^1H/^2D])$ (B) relaxation rates. See the text for details.

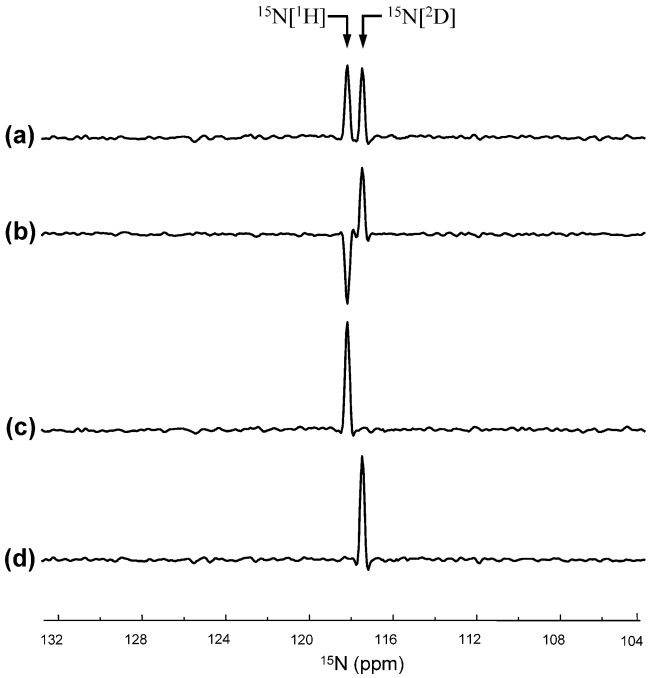

Figure 2. F1(ω_N) traces through the peaks from Glu-27 (proton shift 3.75 ppm, corresponding to $^1H^\alpha$ of the preceding residue; nitrogen shifts 118.2 and 117.5 ppm, corresponding to $^{15}N[^1H]$ and $^{15}N[^2D]$, respectively) extracted from HA(CACO)N[^{1}H/^{2}D] spectra in the R_1 experiment. Traces a and b are from data sets recorded without and with the ^{1}H proton inversion pulse between points d and e in Figure 1, respectively. Traces c and d are generated by subtraction and addition of the original spectra.

speaking, the relaxation of two-spin order, N_zC_z', and antiphase coherence, N_xC_z', is what is measured. In the case of the $R_{1\rho}$ measurement, the relaxation period is flanked by 90°−ξ−90° elements that improve the spin-lock conditions for off-resonance signals.[51,52] Proton 180° pulses are applied during the relaxation period to suppress interference from CSA−dipolar cross-correlation,[53,54] with the number of such pulses, 2*n*, proportional to the duration of the relaxation period, but limited to $2n \leq 6$ to avoid recently described artifacts.[55] Deuterium 180° pulses were applied in some of the experiments to suppress the buildup of $C_z'N_zD_z$ or $C_z'N_xD_z$ that may arise due to ^{15}N CSA, ^{15}N−^{2}D dipolar cross-correlated relaxation. In practice, however, these pulses are not necessary since the latter coherence decays rapidly due to quadrupolar relaxation of the deuteron, leading to a "self-decoupling" effect. Finally, note that under strong spin-lock conditions the scalar relaxation of the second kind in the ^{15}N−^{2}D spin pair is suppressed.[56]

The quality of water suppression is clearly important in these experiments since correlations of interest can be obscured by the water signal that appears in the middle of the spectrum. Water suppression is achieved by means of gradient and rf inhomogeneity dephasing, including Messerle pulses[57] and a gradient−90°−gradient element (preceding point f in the pulse sequence). We have found that still better water suppression can be achieved if the final INEPT transfer step is replaced with a heteronuclear cross-polarization transfer scheme (inset C in Figure 1) since in this case proton irradiation extends right up to the acquisition period. The scheme of inset C, however, adds 3.5 ms

(51) Yamazaki, T.; Muhandiram, R.; Kay, L. E. *J. Am. Chem. Soc.* **1994**, *116*, 8266−8278.
(52) Akke, M.; Palmer, A. G. *J. Am. Chem. Soc.* **1996**, *118*, 911−912.
(53) Palmer, A. G.; Skelton, N. J.; Chazin, W. J.; Wright, P. E.; Rance, M. *Mol. Phys.* **1992**, *75*, 699−711.
(54) Kay, L. E.; Nicholson, L. K.; Delaglio, F.; Bax, A.; Torchia, D. A. *J. Magn. Reson.* **1992**, *97*, 359−375.
(55) Korzhnev, D. M.; Skrynnikov, N. R.; Millet, O.; Torchia, D. A.; Kay, L. E. *J. Am. Chem. Soc.* **2002**, *124*, 10743−10753.
(56) Skrynnikov, N. R.; Lienin, S. F.; Brüschweiler, R.; Ernst, R. R. *J. Chem. Phys.* **1998**, *108*, 7662−7669.
(57) Messerle, B. A.; Wider, G.; Otting, G.; Weber, C.; Wüthrich, K. *J. Magn. Reson.* **1989**, *85*, 608−613.

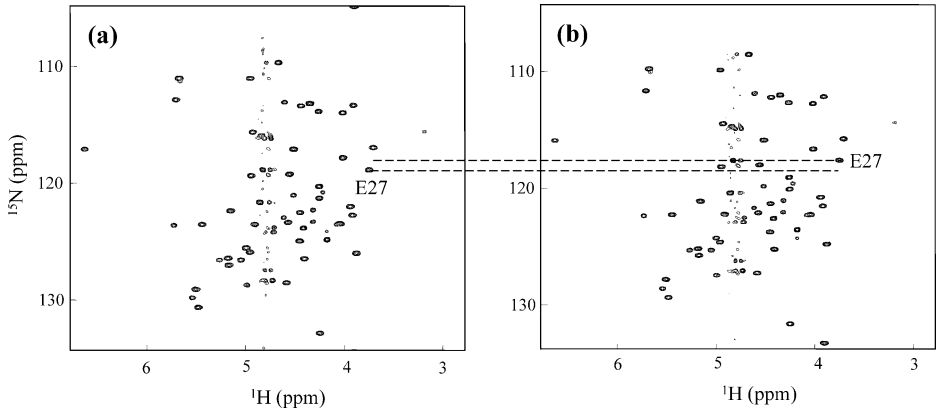

Figure 3. $^{1}H^{\alpha}-^{15}N$ spectral maps from the $R_{1\rho}(C'_zN_x[^1H/^2D])$ experiment recorded on a 1.8 mM sample of protein L, 600 MHz, 26.7 °C. Separation between the $^{15}N[^1H]$ and $^{15}N[^2D]$ signals from residue Glu-27, due to an isotopic shift, is indicated by dotted lines.

to the duration of the sequence and causes a ca. 25% drop in the sensitivity of the experiment in the case of protein L.

As described for other experiments,[58] sample heating can be an issue when a substantial amount of rf power is deposited into the system. We have investigated the degree of sample heating in our measurements using the temperature dependence of the amide ^{15}N chemical shifts. Sample temperature has been determined as a function of the duration of the relaxation period, $4nT$. Increases in temperature of up to 0.2 and 1.0 °C were registered in R_1 and $R_{1\rho}$ experiments, respectively. Simulations establish that differential heating effects of this magnitude introduce a near-constant bias of ~2% in the determined $R_{1\rho}$ rates. This problem can be alleviated by using longer recycling delays or by implementing a heating-compensation scheme.[58]

It is important to point out that both R_1 and $R_{1\rho}$ experiments described above can be compromised if during the relaxation period $^{15}N[^1H]$ is converted into $^{15}N[^2D]$ (and vice versa) due to exchange with solvent. In this case measured relaxation rates represent weighted averages between the "pure" rates from the $^{15}N[^1H]$ and $^{15}N[^2D]$ isotopomers. To determine whether such a situation is present in the case of protein L (pH 5), let us first consider what would be the effect of $^{15}N[^1H]-^{15}N[^2D]$ interconversion on the spectral traces shown in Figure 2.

In the case of Figure 2a, solvent exchange leads to a transfer of *positive* intensity from the $^{15}N[^1H]$ line to the $^{15}N[^2D]$ line. In contrast, when the $^{15}N[^1H]$ line is inverted, Figure 2b, the transferred magnetization is *negative*. The result is that the subtraction of the two traces, Figure 2a,b, fails to completely eliminate the $^{15}N[^2D]$ signal. Thus, if solvent exchange were a factor, we would expect to see a residual signal at the $^{15}N[^2D]$ position in the trace of Figure 2c (likewise, a residual $^{15}N[^1H]$ signal would appear in Figure 2d). In fact, no such signals are observed (see Figure 2c,d), even for the longest relaxation delays (0.8 s in R_1 measurements). This clearly indicates that any effects from exchange with solvent are below the noise level in the current set of experiments.

Pulse Sequence Details. Figure 1 shows the pulse sequences for measuring longitudinal $R_1(C'_zN_z[^1H/^2D])$ (A) and transverse $R_{1\rho}(C'_zN_x[^1H/^2D])$ (B) relaxation rates. All narrow (wide) pulses (irrespective of height) are applied with a flip angle of 90° (180°) along the *x*-axis unless indicated otherwise. The ^1H rf carrier is set at 4.77 ppm. ^1H pulses are applied with an rf field strength of 51 kHz (600 MHz), with the exception of the two consecutive water purge pulses[57] (open rectangles, durations of 6.0 and 3.7 ms) that use a field of 12.4 kHz and ^1H WALTZ-16 decoupling, which employs a field of 6.5 kHz. The 180° rectangular ^1H pulse between points d and e (dotted outline) is executed in alternate scans. The ^{13}C rf carrier is originally positioned at 58 ppm, at point c jumped to 176 ppm, and at point f returned to 58 ppm. ^{13}C pulses applied during the first and last INEPT elements use a 16 kHz field, while the remaining rectangular ^{13}C 90° (180°) pulses are applied with a field strength of $\Delta/\sqrt{15}$ ($\Delta/\sqrt{3}$), where Δ is the frequency offset (Hz) between the $^{13}C^{\alpha}$ and $^{13}C'$ spectral regions (118 ppm). The shaped ^{13}C pulse in the center of the t_1 period has the WURST profile[59] (maximum field strength of 11.4 kHz, duration of 400 μs, centered at 116 ppm; the pulse is shown on all three ^{13}C channels to indicate its broad-band character). The $^{13}C^{\beta}$ pulses (filled shapes) are of the I-BURP2 variety[60] (at 600 MHz: maximum field strength 3.25 kHz, duration 1.54 ms, excitation bandwidth 17 ppm, centered at 30 ppm). $^{13}C^{\alpha}$ decoupling during acquisition is accomplished by a WALTZ-16 sequence with a 2.3 kHz field strength. The pulses marked with "BS" compensate for Bloch−Siegert shifts.[61] All ^{15}N pulses are applied with the rf carrier at 119 ppm and a 6.3 kHz rf field. The strength of the spin-lock field (inset B) is 1.7 kHz. The ^2H rf carrier is set at 8.3 ppm; deuterium pulses and WALTZ-16 decoupling are applied with field strengths of 2.3 and 0.74 kHz, respectively. The delays used are $\tau_a = \tau_b = 1.8$ ms, $\tau_c = 4$ ms, $\tau_d = 12$ ms, $\tau_e = 2.7$ ms, and $\xi = 40$ μs (see ref 51 for calculation of ξ). The phase cycle employed in the R_1 experiment is $\phi_1 = 2x, 2(-x)$, $\phi_2 = 8x, 8(-x)$, $\phi_3 = (x, -x)$, $\phi_4 = 4x, 4(-x)$, rec = $(x, -x, -x, x), 2(-x, x, x, -x), (x, -x, -x, x)$, whereas in the $R_{1\rho}$ experiment the phase cycle employed is $\phi_1 = 2x, 2(-x)$, $\phi_2 = x$, $\phi_3 = 4x, 4(-x)$, $\phi_4 = 8x, 8(-x)$, $\phi_5 = (y, -y)$, rec = $(x, -x, -x, x), 2(-x, x, x, -x), (x, -x, -x, x)$. Quadrature detection in t_1 is accomplished by States-TPPI[62] of ϕ_4. The strengths and durations of the gradients are (g1) 0.5 ms, 8 G/cm, (g2) 0.2 ms, 4 G/cm, (g3) 1 ms, 15 G/cm, (g4) 0.4 ms, 12 G/cm, (g5) 0.6 ms, 14 G/cm, (g6) 0.3 ms, 10 G/cm, (g7) 0.25 ms, 30 G/cm, (g8) 0.3 ms, 16 G/cm, (g9) 3.5 ms, 20 G/cm, (g10) 2 ms, 20 G/cm, (g11) 0.3 ms, 12 G/cm, and (g12) 0.2 ms, 10 G/cm. Inset C shows the heteronuclear cross-polarization scheme (DIPSI-3, 7.8 kHz ^1H and ^{13}C fields, duration 7 ms) for transferring magnetization from $^{13}C^{\alpha}$ to $^1H^{\alpha}$. This element replaces the main scheme starting from point g.

NMR Data. $^{1}H^{\alpha}-^{15}N$ planes from $R_{1\rho}(C'_zN_x[^1H])$ and $R_{1\rho}(C'_zN_x[^2D])$ measurements (duration of relaxation period 2 ms) are shown in parts a and b, respectively, of Figure 3. The data were recorded in an interleaved manner, as described above, in a total time of 3 h and 40 min, 600 MHz, 26.7 °C. Data sets were collected as 128 × 154 complex matrices with acquisition times of 71 and 64 ms in t_1 and t_2. The FID corresponding to the first t_1 increment in each data set was multiplied by a factor of 1.5 since the starting t_1 value was set equal to one dwell time.[63] The phase corrections in the indirect dimension were (−180°, 360°). Spectra were processed using nmrPipe[64] with a first-order polynomial filter for water suppression.

(58) Wang, A. C.; Bax, A. *J. Biomol. NMR* **1993**, *3*, 715−720.
(59) Kupce, E.; Freeman, R. *J. Magn. Reson. Ser. A* **1995**, *115*, 273−276.
(60) Geen, H.; Freeman, R. *J. Magn. Reson.* **1991**, *93*, 93−141.
(61) Vuister, G. W.; Bax, A. *J. Magn. Reson.* **1992**, *98*, 428−435.
(62) Marion, D.; Ikura, M.; Tschudin, R.; Bax, A. *J. Magn. Reson.* **1989**, *85*, 393−399.
(63) Zhu, G.; Torchia, D. A.; Bax, A. *J. Magn. Reson., Ser. A* **1993**, *105*, 219−222.

$^1H^{\alpha}-^{15}N$ correlation maps are remarkably free of overlap (by contrast, four pairs of heavily overlapped peaks are noted in the standard $^1H^N-^{15}N$ HSQC map). At 600 MHz, relaxation rates were obtained for 56 residues out of 63. Missing are all residues following glycines (4), residues giving rise to very weak peaks (2), and one residue for which the $^1H^{\alpha}$ assignment was not confirmed (1). The nine peaks within ±0.1 ppm of the water signal were all selected for analysis. For these peaks, however, the average R_1 and $R_{1\rho}$ error was 5.1%, compared to 2.1% for the rest of the peaks (the errors were derived from Monte Carlo analyses implemented in the exponential fitting routine). The level of water suppression obtained in data sets recorded at 500 MHz was inferior to that at 600 MHz, and as a consequence, only 50 residues were selected for analysis; specifically, the six peaks falling within ±0.1 ppm of the water line were not used.

Of interest, the signal-to-noise ratio in $^1H^{\alpha}-^{15}N[^2D]$ spectra is 90% of that in the corresponding $^1H^{\alpha}-^{15}N[^1H]$ data sets (compare, for example, parts c and d of Figure 2). This observation is somewhat unexpected. Considering the slight preference of amide groups for deuterium[65] and taking into account relaxation losses (protonated amides experience higher losses, especially during the period d−e in the pulse sequence), one expects this ratio to be on the order of 1.15. It is clear that the composition of the solvent slightly deviates from a 50:50 mixture of H_2O and D_2O. The intensities observed in the spectra are consistent with a 56:44 composition. Indeed, a small excess of protons over deuterons in the solvent was confirmed by electron-impact mass spectrometry.

Conventional ^{15}N R_1, $R_{1\rho}$, steady-state NOE experiments (referred to in what follows as $R_1(N_z[^1H])$, $R_{1\rho}(N_x[^1H])$, and $NOE(N_z,H_z)$) were recorded using the sensitivity-enhanced sequences of Farrow et al.[66] The schemes of Figure 1 are about 5 times less sensitive than these conventional (sensitivity-enhanced) experiments, recorded with identical acquisition times, and therefore, their use is restricted to applications involving sensitive samples.

All spectra were processed using the nonlinear spectral line shape fitting procedure nlinLS from the nmrPipe software package.[64] The decay curves obtained from the peak volumes were fitted to a single exponential; the quality of the fits for "typical" residues is illustrated in Figure 4 (the choice of the three typical residues is explained later). The decay curves from all experiments and for all residues, except the terminal residue Glu-2, were well fit to a single exponential. In the case of Glu-2, the decay curves were strongly biexponential; this residue was therefore excluded from all further analyses.

$R_1(C_z'N_z[^1H])$ and $R_{1\rho}(C_z'N_x[^1H])$ rates were compared with values measured independently using HNCO-based relaxation experiments[67] (this is obviously possible only for protonated and not for deuterated amide groups). In the case of R_1 rates, the standard rms deviation between the two independent data sets is 3.8%, with a mean deviation of 0.4%. In the case of $R_{1\rho}$, the standard rms deviation is 5.5%, with a mean deviation of 5.4%, suggesting the presence of a subtle bias. The origin of this bias remains unclear. It is likely, however, that this bias equally affects $R_{1\rho}(C_z'N_x[^1H])$ and $R_{1\rho}(C_z'N_x[^2D])$ data (this would be the case, for example, if it is caused by hardware limitations[68]). If this is the case, then the bias will be eliminated by evaluating the difference $R_2(C_z'N_x[^1H]) - R_2(C_z'N_x[^2D])$. This is the differential relaxation rate that is used in the analysis below.

Results and Discussion

Relaxation Rates. Figure 5 shows the measured $R_1(C_z'N_z[^1H])$, $R_1(C_z'N_z[^2D])$, $R_2(C_z'N_x[^1H])$, and $R_2(C_z'N_x[^2D])$ rates as a function of residue number in protein L. The variations in the measured rates reflect anisotropic tumbling of the protein and variations in the local order parameters S^2. The data generally follow the same pattern for protonated and deuterated amides (filled and empty symbols, respectively). This is not surprising since these two data sets are (essentially) different only with regard to $^{15}N-^1H/^{15}N-^2D$ dipolar interactions. Furthermore, $^{15}N-^1H$ and $^{15}N-^2D$ vectors sense anisotropic tumbling and local fluctuations in a similar manner.

The direct interpretation of $C_z'N_z$ and $C_z'N_x$ relaxation rates in terms of dynamics parameters is feasible, but not appealing. The sizable relaxation contribution from the carbonyl CSA mechanism introduces an additional degree of uncertainty in comparison to traditional ^{15}N relaxation studies.[35,69] Furthermore, the carbonyl spin may well sample local dynamics

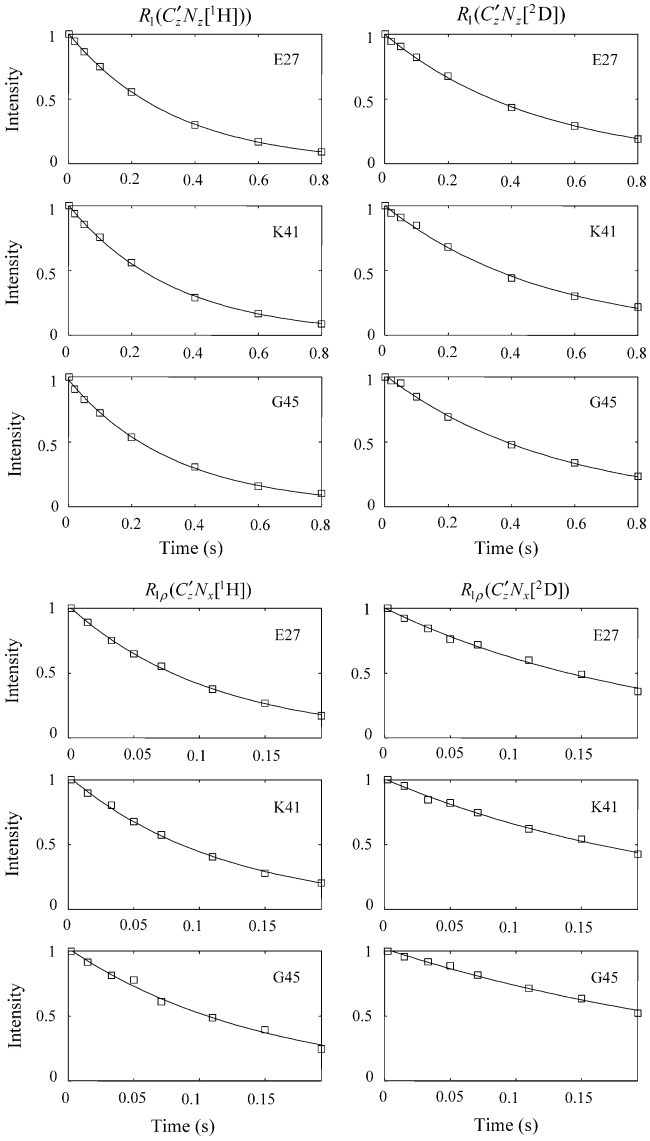

Figure 4. Relaxation decay curves $R_1(C_z'N_z[^1H/^2D])$ and $R_{1\rho}(C_z'N_x[^1H/^2D])$ for selected residues (600 MHz). R_2 rates were obtained from $R_{1\rho}$ and R_1, taking into account off-resonance effects.[66] The uncertainty for the data shown is less or equal to the height of the square symbols in the plot (estimated from the effect of spectral noise on peak volumes determined by the program nlinLS[64]).

(64) Delaglio, F.; Grzesiek, S.; Vuister, G. W.; Zhu, G.; Pfeifer, J.; Bax, A. *J. Biomol. NMR* **1995**, *6*, 277−293.
(65) LiWang, A. C.; Bax, A. *J. Am. Chem. Soc.* **1996**, *118*, 12864−12865.
(66) Farrow, N. A.; Muhandiram, R.; Singer, A. U.; Pascal, S. M.; Kay, C. M.; Gish, G.; Shoelson, S. E.; Pawson, T.; Forman-Kay, J. D.; Kay, L. E. *Biochemistry* **1994**, *33*, 5984−6003.
(67) Dayie, K. T.; Wagner, G. *J. Am. Chem. Soc.* **1997**, *119*, 7797−7806.
(68) Guenneugues, M.; Berthault, P.; Desvaux, H. *J. Magn. Reson.* **1999**, *136*, 118−126.
(69) Lienin, S. F.; Bremi, T.; Brutscher, B.; Brüschweiler, R.; Ernst, R. R. *J. Am. Chem. Soc.* **1998**, *120*, 9870−9879.

differently from the nitrogen spin.[69] Therefore, we choose to consider the *differences* between the rates measured in the protonated and deuterated groups.

By evaluating $R_1(C_z'N_z[^1H]) - R_1(C_z'N_z[^2D])$ and $R_2(C_z'N_x[^1H]) - R_2(C_z'N_x[^2D])$, a number of relaxation contributions are eliminated. In particular, carbonyl and nitrogen CSA contributions, chemical exchange (R_{ex}), and minor terms arising from dipolar interactions involving either external protons or adjacent carbons are subtracted out. In addition, experimental artifacts that affect both $C_z'N_x[^1H]$ and $C_z'N_x[^2D]$ (or $C_z'N_z[^1H]$ and $C_z'N_z[^2D]$) data in the same way can be removed in this manner, as commented in the previous section.

The difference in relaxation rates measured for the $^{15}N-^{1}H$ and $^{15}N-^{2}H$ spin pairs can be accounted for, to excellent approximation, by the difference in the respective dipolar interactions:

$$R_1(C_z'N_z[^1H]) - R_1(C_z'N_z[^2D]) = \frac{1}{12}\left(\frac{\mu_0}{4\pi}\right)^2\left(\frac{\gamma_H\gamma_N\hbar}{r_{NH}^3}\right)^2\{J(\omega_H - \omega_N) + 3J(\omega_N) + 6J(\omega_H + \omega_N)\} - \frac{2}{9}\left(\frac{\mu_0}{4\pi}\right)^2\left(\frac{\gamma_D\gamma_N\hbar}{r_{ND}^3}\right)^2\{J(\omega_D - \omega_N) + 3J(\omega_N) + 6J(\omega_D + \omega_N)\} \quad (2a)$$

$$R_2(C_z'N_x[^1H]) - R_2(C_z'N_x[^2D]) = \frac{1}{24}\left(\frac{\mu_0}{4\pi}\right)^2\left(\frac{\gamma_H\gamma_N\hbar}{r_{NH}^3}\right)^2\{4J(0) + J(\omega_H - \omega_N) + 3J(\omega_N) + 6J(\omega_H) + 6J(\omega_H + \omega_N)\} - \frac{1}{9}\left(\frac{\mu_0}{4\pi}\right)^2\left(\frac{\gamma_D\gamma_N\hbar}{r_{ND}^3}\right)^2\{4J(0) + J(\omega_D - \omega_N) + 3J(\omega_N) + 6J(\omega_D) + 6J(\omega_D + \omega_N)\} \quad (2b)$$

The symbols used in eq 2 are standard,[66] with the spectral densities defined such that in the limit of an isotropically tumbling rigid molecule $J(\omega) = (1/5)\tau_R/(1 + \omega^2\tau_R^2)$.

In eq 2, pairs of different relaxation parameters, $R_1(C_z'N_z[^1H])$ and $R_1(C_z'N_z[^2D])$, $R_2(C_z'N_x[^1H])$ and $R_2(C_z'N_x[^2D])$, are combined with the aim of simplifying the interpretation of the data. Such an approach has been extensively used in the past,[70−73] with perhaps the most important example being the spectral density mapping methodology of Peng and Wagner.[74] In our case, combining the two measured rates leads to a dramatic simplification of the analysis as demonstrated by eq 2: the expression is limited to a pair of simple dipolar terms. Furthermore, these two dipolar terms refer to the same nitrogen−hydrogen bond vector so that essentially no additional spectroscopic, structural, or dynamic parameters are involved when the combination in eq 2 is formed. It should be noted, however, that, in addition to the leading contribution given by eq 2, the differences $R_1(C_z'N_z[^1H]) - R_1(C_z'N_z[^2D])$ and $R_2(C_z'N_x[^1H]) - R_2(C_z'N_x[^2D])$ include a small term arising from $^{13}C'-^{1}H^N$ and $^{13}C'-^{2}D^N$ dipolar interactions. The expression for this extra term can be obtained by a trivial substitution in eq 2a where N is replaced by C′; this term is identical for $R_1(C_z'N_z[^1H]) - R_1(C_z'N_z[^2D])$ and $R_2(C_z'N_x[^1H]) - R_2(C_z'N_x[^2D])$ rates. In the case of protein L, this correction adds 2.9% and 0.7% to the rates listed in eqs 2a and 2b, respectively. In subsequent analyses, these small terms are rigorously taken into account, including the effect of anisotropic tumbling on each $C'-H^N$ vector.

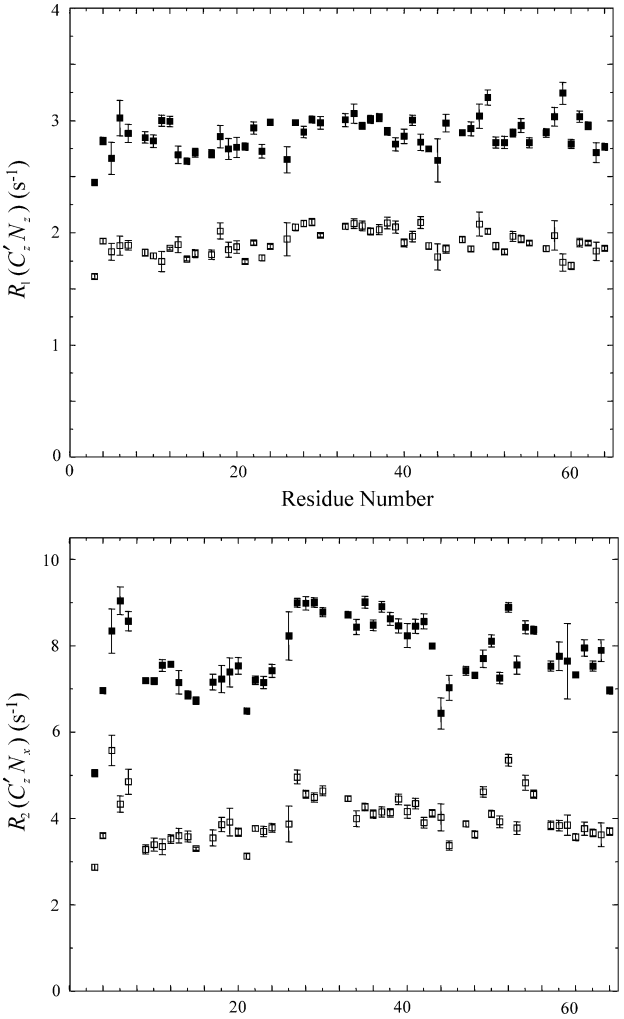

Figure 5. Relaxation rate constants for protein L, 600 MHz, 26.7 °C, plotted as a function of residue number: $R_1(C_z'N_z[^1H])$ and $R_2(C_z'N_x[^1H])$ (filled squares), $R_1(C_z'N_z[^2D])$ and $R_2(C_z'N_x[^2D])$ (open squares).

Certain assumptions are necessary for the interpretation of relaxation rates, eq 2, in terms of dynamics. First, we assume that the local dynamics of the peptide plane does not change when an amide proton is substituted by a deuteron. Given that the increment in mass is small, this seems reasonable. Second, we assume that $r_{NH} = r_{ND}$. In fact, deuteration leads to a slight reduction in the effective length of the bond. For example, r_{CD} is ca. 0.005 Å shorter than r_{CH}.[75] While the data on amides are not available, the relatively small size of the $^{15}N[^1H/^2D]$ isotopic shift, 0.7 ppm, suggests that the reduction in bond length is similarly small (see, for example, ref 76). A study of proton/

(70) Lee, L. K.; Rance, M.; Chazin, W. J.; Palmer, A. G. *J. Biomol. NMR* **1997**, *9*, 287−298.
(71) Fushman, D.; Tjandra, N.; Cowburn, D. *J. Am. Chem. Soc.* **1998**, *120*, 10947−10952.
(72) Muhandiram, D. R.; Yamazaki, T.; Sykes, B. D.; Kay, L. E. *J. Am. Chem. Soc.* **1995**, *117*, 11536−11544.
(73) Phan, I. Q. H.; Boyd, J.; Campbell, I. D. *J. Biomol. NMR* **1996**, *8*, 369−378.
(74) Peng, J. W.; Wagner, G. *J. Magn. Reson.* **1992**, *98*, 308−332.
(75) Raynes, W. T.; Fowler, P. W.; Lazzeretti, P.; Zanasi, R.; Grayson, M. *Mol. Phys.* **1988**, *64*, 143−162.

deuteron vibrational states involving both stretching and wagging modes is currently under way.

It is important to note that, contrary to what one may expect, the deuteron is not a "silent" nucleus in these new relaxation experiments.[77] Despite the low gyromagnetic ratio of a deuteron in relation to a proton, the $^{15}N-^{2}D$ dipolar relaxation rate amounts to ca. 33% of the corresponding $^{15}N-^{1}H$ rate, as calculated from eq 2a (600 MHz) for longitudinal relaxation rates using the dynamic parameters of protein L. Two factors are responsible for this relatively large contribution. First, as reflected in eq 2, the rates are proportional to $S(S+1)$, where S is the spin quantum number of hydrogen (1 for deuterium, 1/2 for proton).[78] Second, the spectral densities $J(\omega_D \pm \omega_N)$ are much larger than $J(\omega_H \pm \omega_N)$ because they involve much lower frequencies. In the case of transverse relaxation, both $^{15}N-^{1}H$ and $^{15}N-^{2}D$ rates are dominated by $J(0)$ and the $^{15}N-^{2}D$ rates are, therefore, less significant (ca. 15% of the $^{15}N-^{1}H$ rates).

Protein Tumbling. The ratio of ^{15}N relaxation rates $R_2(N_x[^1H])/R_1(N_z[^1H])$ has been widely used to characterize overall tumbling of proteins.[70,79,80] We have carried out an R_2/R_1 analysis using an optimization program written in-house. Combined data from conventional ^{15}N measurements at 500 and 600 MHz were employed. $^{1}H-^{15}N$ dipolar and ^{15}N CSA interactions were taken into account in the treatment, with a value of -172 ppm used for the nitrogen CSA[81] and 20° for the angle between the long axis of the CSA tensor and the NH bond.[35] A single residue, Glu-3, displaying a negative NOE(N_z,H_z) value, was excluded from this analysis. The errors in the output parameters were evaluated by means of a jackknife procedure discarding at random 20% of the input data.

The relaxation data are best fit to a model which assumes axially symmetric anisotropic diffusion (a more complex treatment involving a fully anisotropic diffusion tensor is not warranted[82]). The following values were obtained for the components of the diffusion tensor: $D_{iso} = (3.73 \pm 0.01) \times 10^7\ s^{-1}$, $D_\parallel/D_\perp = 1.44 \pm 0.02$. These results are very similar to those obtained using the program R2R1_diffusion,[83] with the 500 and 600 MHz data sets analyzed separately. Previously, D_{iso} and $D_\parallel/D_\perp$ values of $4.11 \times 10^7\ s^{-1}$ and 1.43 were reported for protein L dissolved in a 90% $H_2O-10\%$ D_2O mixture.[82] The difference between the two D_{iso} values is in line with expectations considering the increased viscosity of solvent containing a higher proportion of D_2O.[65]

It is also possible to obtain diffusion parameters from the relaxation rates that are measured in the present set of experiments. We have used the ratio $\{R_2(C_z'N_x[^1H]) - R_2(C_z'N_x[^2D])\}/\{R_1(C_z'N_z[^1H]) - R_1(C_z'N_z[^2D])\}$ to determine the diffusion tensor. The same algorithm was used as for conventional ^{15}N relaxation data; the calculations were based on eq 2 supplemented with Woessner's formula for $J(\omega)$ for axially symmetric rotational diffusion.[84] Diffusion parameters $D_{iso} = (3.83 \pm 0.02) \times 10^7\ s^{-1}$ and $D_\parallel/D_\perp = 1.52 \pm 0.03$ were obtained when data from both 500 and 600 MHz were combined; values of $(3.79 \pm 0.02) \times 10^7\ s^{-1}$ and 1.48 ± 0.04 were calculated when only 600 MHz data were used. These values are in close agreement with those obtained using the conventional R_2/R_1 ratios (the slight differences in D_{iso} values are consistent with a small amount of sample heating in our measurements). Furthermore, the long axis of the diffusion tensor determined in this analysis is within $9 \pm 3°$ of the axis found using the conventional approach.

It is worth mentioning that the above analyses included a number of minor relaxation contributions that were discussed in the previous section. In particular, in the case of $\{R_2(C_z'N_x[^1H]) - R_2(C_z'N_x[^2D])\}/\{R_1(C_z'N_z[^1H]) - R_1(C_z'N_z[^2D])\}$, the small difference terms associated with the $^{13}C'-^{1}H^N/^{13}C'-^{2}D^N$ interactions have been included. For the $R_2(N_x[^1H])/R_1(N_z[^1H])$ ratio we have considered contributions from dipolar interactions of ^{15}N with $^{13}C'$, $^{13}C^\alpha$, and external ^{1}H spins (in principle, other minor terms might also be present). In all cases these additional effects are essentially inconsequential: they are responsible for a ca. 1% change in D_{iso} and vanishingly small changes in the orientation of the long axis.

The good agreement between diffusion parameters obtained using the two methods described above (i) provides confidence in the new methodology and (ii) confirms the already known fact that the traditional R_2/R_1 analysis is robust, despite the assumptions concerning CSA values, potential R_{ex} contributions, and minor relaxation terms. These assumptions are, of course, avoided in the $^{15}N-^{1}H/^{15}N-^{2}D$ relaxation difference method, although at the expense of lower sensitivity (see above). On the other hand, the new method remains sensitive to a possible effect of intermediate time scale (~1 ns) internal motions on the analysis of overall tumbling.

Local Dynamics. In the preceding section we verified that $R_1(N_z[^1H])$, $R_2(N_x[^1H])$ and $R_1(C_z'N_z[^1H/^2D])$, $R_2(C_z'N_x[^1H/^2D])$ rates provide a consistent picture of overall tumbling for protein L. In the present section we demonstrate that there is also good agreement with respect to local dynamics. This can be established in a number of ways. In particular, for each individual residue the experimentally determined differences $R_1(C_z'N_z[^1H]) - R_1(C_z'N_z[^2D])$ and $R_2(C_z'N_x[^1H]) - R_2(C_z'N_x[^2D])$ can be used to extract the order parameter and local correlation time, S^2 and τ_e, using the Lipari–Szabo model.[85] (Note that R_{ex} contributions are absent from the difference in transverse rates above). Here we adopt a somewhat different approach. Specifically, we use S^2 and τ_e obtained from conventional data to *back-calculate* the new rates. The following three-step algorithm is used for this purpose.

(i) The overall diffusion tensor is determined from $R_2(N_x[^1H])/R_1(N_z[^1H])$ ratios, as described above.

(ii) $R_1(N_z[^1H])$, $R_2(N_x[^1H])$, and NOE(N_z,H_z) data are used to extract S^2, τ_e, and R_{ex} on a per-residue basis, with data from 500 and 600 MHz fitted simultaneously using the rotational diffusion parameters determined in step i. Overall, the procedure is similar to that used in the program Modelfree by Palmer and

(76) Benedict, H.; Hoelger, C.; Aguilar-Parrilla, F.; Fehlhammer, W. P.; Wehlan, M.; Janoschek, R.; Limbach, H. H. *J. Mol. Struct.* **1996**, *378*, 11–16.
(77) Ishima, R.; Petkova, A. P.; Louis, J. M.; Torchia, D. A. *J. Am. Chem. Soc.* **2001**, *123*, 6164–6171.
(78) Abragam, A. *The Principles of Nuclear Magnetism*; Clarendon Press: Oxford, 1961.
(79) Tjandra, N.; Feller, S. E.; Pastor, R. W.; Bax, A. *J. Am. Chem. Soc.* **1995**, *117*, 12562–12566.
(80) Tsan, P.; Hus, J. C.; Caffrey, M.; Marion, D.; Blackledge, M. *J. Am. Chem. Soc.* **2000**, *122*, 5603–5612.
(81) Kroenke, C. D.; Rance, M.; Palmer, A. G. *J. Am. Chem. Soc.* **1999**, *121*, 10119–10125.
(82) Skrynnikov, N. R.; Millet, O.; Kay, L. E. *J. Am. Chem. Soc.* **2002**, *124*, 6449–6460.
(83) Mandel, A. M.; Akke, M.; Palmer, A. G. *J. Mol. Biol.* **1995**, *246*, 144–163.
(84) Woessner, D. E. *J. Chem. Phys.* **1962**, *37*, 647–654.
(85) Lipari, G.; Szabo, A. *J. Am. Chem. Soc.* **1982**, *104*, 4546–4559.

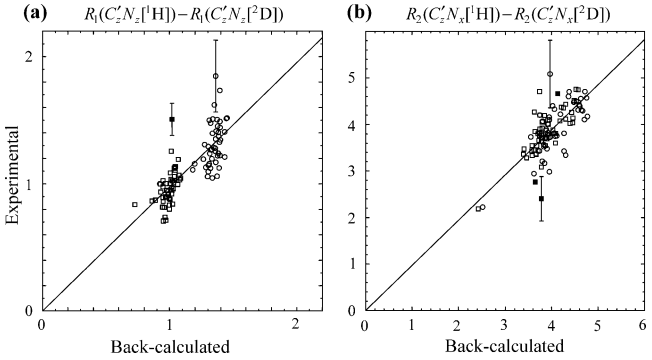

Figure 6. Experimentally determined difference rates $R_1(C'_zN_z[^1H]) - R_1(C'_zN_z[^2D])$ and $R_2(C'_zN_x[^1H]) - R_2(C'_zN_x[^2D])$ vs values back-calculated on the basis of conventional $R_1(N_z[^1H])$, $R_2(N_x[^1H])$, and NOE(N_z,H_z) data. Filled squares correspond to the peaks for which $^1H^\alpha$ frequencies fall within ±0.1 ppm of the water signal. The two worst outliers in each graph are shown together with their respective error bars. The straight lines are obtained from the least-squares fitting of all points to the equation $y = ax$.

co-workers.[83] The calculation of relaxation parameters in this procedure uses Woessner's expression for a spectral density function that is appropriate for axially symmetric rotation and accounts for local dynamics via the Lipari−Szabo model.[85] Although combining anisotropic tumbling with the Lipari−Szabo model is not rigorous,[86] this approach has been shown to be perfectly reasonable for most biomolecular applications.[85] The analysis takes into account the ^{15}N CSA interaction, ^{15}N dipolar interactions with $^1H^N$ and other proximal protons (as determined from the X-ray structure of protein L[46]), and interactions with the adjacent $^{13}C^\alpha$ and $^{13}C'$ carbons. In addition, exchange terms have been included in the $R_2(N_x[^1H])$ rates, assuming that R_{ex} scales with the square of the magnetic field B_0 (this assumption seems reasonable since only small exchange terms associated with microsecond time-scale motion are possibly present in protein L). The inclusion of minor relaxation channels at this stage of the analysis is important (see below).

(iii) The rotational diffusion parameters determined in step i together with S^2 and τ_e values computed on a per-residue basis in step ii are used to calculate $R_1(C'_zN_z[^1H]) - R_1(C'_zN_z[^2D])$ and $R_2(C'_zN_x[^1H]) - R_2(C'_zN_x[^2D])$. The calculations are based on eq 2, using the form of $J(\omega)$ described above. In addition to the dominant terms listed in eq 2, the small contributions from $^{13}C'-^1H^N/^{13}C'-^2D^N$ interactions are also included in the calculated rates.

The values of $R_1(C'_zN_z[^1H]) - R_1(C'_zN_z[^2D])$ and $R_2(C'_zN_x[^1H]) - R_2(C'_zN_x[^2D])$ and calculated in this manner are subsequently compared with the experimental results, Figure 6. Both 500 and 600 MHz data sets are included in the comparison, and no residues are omitted. The plots show a fairly good degree of correlation, with the scatter reflecting mainly the limited signal-to-noise ratio of the new experiments. Note that random errors increase when the differences between two experimentally determined rates, $R_1(C'_zN_z[^1H]) - R_1(C'_zN_z[^2D])$ and $R_2(C'_zN_x[^1H]) - R_2(C'_zN_x[^2D])$, are evaluated. The worst outliers from each data set are shown in the figure together with their respective error bars (the errors are derived as part of the exponential fitting of the experimental relaxation curves; in our past experience, the errors obtained in this manner are somewhat underestimated). As expected, the scatter is more pronounced in the 500 MHz data (circles), reflecting the decreased signal-to-noise ratio relative to that of data recorded at 600 MHz. Among the 600 MHz data (squares), most of the outliers correspond to peaks that fall within ±0.1 ppm of the water resonance and are, therefore, somewhat compromised by the residual water signal (filled squares). However, a certain fraction of the scatter is likely due to a meaningful difference between the experimental and calculated rates. These differences reflect the uncertainties intrinsic to the analysis of conventional R_1, R_2, NOE data that are associated, for example, with nitrogen CSA and R_{ex} contributions.

The spread of the points in the graph of longitudinal relaxation rates, Figure 6a, is mainly due to the dependence on the static magnetic field, while in the case of transverse rates, Figure 6b, the spread mainly reflects the anisotropy of tumbling, $D_\parallel/D_\perp = 1.44$. Both these features are predicted by eq 2 for a protein tumbling with $\tau_R = 1/(6D_{iso}) = 4.47$ ns. The straight lines drawn in Figure 6 are obtained from least-squares fits of all points (i.e., 500 and 600 MHz data) to the equation $y = ax$, with slope a equal to 0.98 and 0.97 in Figures 6a and 6b, respectively. Of interest, when the minor dipolar relaxation mechanisms are not included in the analysis of the conventional relaxation data, step ii, the order parameters are overestimated and, consequently, slopes of 0.92 and 0.91 are obtained for the correlations in Figure 6. In general, if a comparison between different types of relaxation data is intended, an effort should be made to account for all relaxation channels.[69]

Including additional relaxation mechanisms in step ii above (such as, for example, contributions from the antisymmetric component of the CSA tensor and relaxation from solvent) would lead to an increase in the slopes from 0.97−0.98 toward 1.00. A similar effect would be obtained if a slightly shorter value of the bond length r_{ND} was used in step iii. However, the magnitude of these additional corrections remains uncertain, and in any event, we do not feel that the precision of our data justifies their inclusion. Finally, noting that the $R_2(C'_zN_x[^1H/^2D])$ measurements deposit more heat to the sample than the conventional experiments, we have repeated the analysis above using a value of $D_{iso} = 3.83 \times 10^7\ s^{-1}$ in steps ii and iii (see the previous section), which resulted in a slope of 0.99 in Figure 6b.

Spectral Density Mapping. In the previous two sections it has been demonstrated that the new relaxation rates $R_1(C'_zN_z[^1H/^2D])$ and $R_2(C'_zN_x[^1H/^2D])$ are compatible with the results of the standard ^{15}N experiments, $R_1(N_z[^1H])$, $R_2(N_x[^1H])$, and NOE(N_z,H_z). We now combine the data from the new and conventional experiments with the aim to sample the spectral density function at frequencies below those that are available from conventional ^{15}N experiments alone. In what follows we will use a spectral density mapping procedure[74] which allows the extraction of $J(\omega)$ values at characteristic frequencies without resorting to any assumptions about the nature of the motion. In particular, spectral densities evaluated at low frequencies ω can be essential for characterizing local motions on a nanosecond time scale (typical for flexible backbone fragments and for side chains).[82,87−89]

Equation 2a contains a pair of terms that are unique to the new experiments considered here, $6J(\omega_D + \omega_N)$ and

(86) Daragan, V. A.; Mayo, K. H. *J. Phys. Chem. B* **1999**, *103*, 6829−6834.
(87) Buevich, A. V.; Baum, J. *J. Am. Chem. Soc.* **1999**, *121*, 8671−8672.
(88) Idiyatullin, D.; Daragan, V. A.; Mayo, K. H. *J. Magn. Reson.* **2001**, *152*, 132−148.
(89) Roberts, M. F.; Cui, Q. Z.; Turner, C. J.; Case, D. A.; Redfield, A. G. *Biochemistry* **2004**, *43*, 3637−3650.

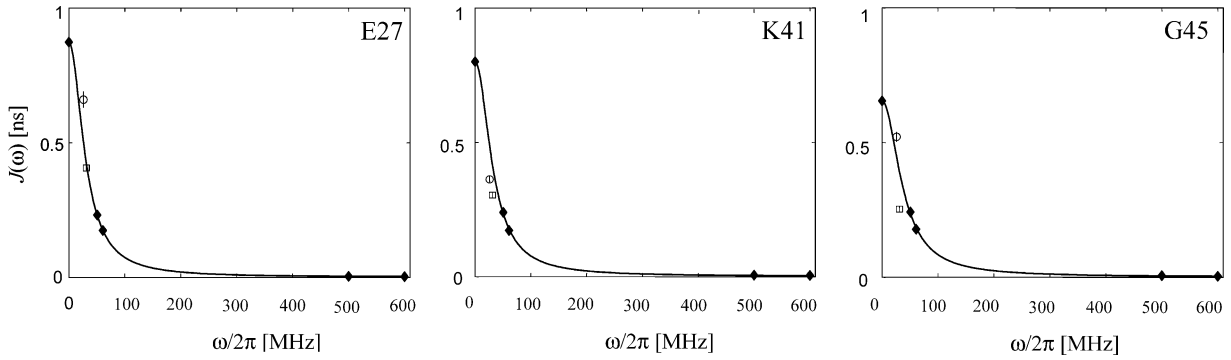

Figure 7. Spectral densities $J(\omega)$ for residues Glu-27, Lys-41, and Gly-45 in protein L. The values of $J(0)$, $J(\omega_N)$, $J(\omega_H)$ obtained from analyses of conventional $R_1(N_z[^1H])$, $R_2(N_x[^1H])$, and NOE(N_z,H_z) data recorded at 500 and 600 MHz are indicated by filled diamonds. The continuous curves are obtained from three-parameter Lipari−Szabo[85] fits of these five points. The values of $J(\omega_D + \omega_N)$ extracted from $R_1(C_z'N_z[^1H]) - R_1(C_z'N_z[^2D])$ measured at 500 and 600 MHz are displayed with open circles and squares, respectively.

$J(\omega_D - \omega_N)$. Of note, due to the negative gyromagnetic ratio of nitrogen, the term $6J(\omega_D + \omega_N)$ samples a very low frequency (equal to almost exactly half of ω_N). Calculations described in the previous section establish that for protein L $J(\omega_D - \omega_N)$ is, on average, less than 2% of $6J(\omega_D + \omega_N)$ and can, therefore, be neglected. Since other spectral densities, $J(\omega_H \pm \omega_N)$ and $J(\omega_N)$, can be evaluated from the analysis of conventional ^{15}N relaxation data, the value of $6J(\omega_D + \omega_N)$ can be obtained directly from the experimentally measured difference $R_1(C_z'N_z[^1H]) - R_1(C_z'N_z[^2D])$.

To arrive at values for $J(\omega_H \pm \omega_N)$ and $J(\omega_N)$, spectral density mapping was performed using a data set comprised of $R_1(N_z[^1H])$, $R_2(N_x[^1H])$, and NOE(N_z,H_z) values measured at two fields (six pieces of data) and assuming that $J(\omega_H \pm \omega_N) = J(\omega_H)$.[90,91] (More sophisticated approaches where linear combinations involving $J(\omega_H \pm \omega_N)$ and $J(\omega_H)$ were replaced with $J(\beta\omega_H)$ with specially adjusted coefficients β[92] did not lead to any improvements in data fitting.) Values for $J(\omega_N)$ and $J(\omega_H)$ evaluated at $\omega_N/2\pi = 50$ and 60 MHz and $\omega_H/2\pi = 500$ and 600 MHz, in addition to $J(0)$ (total of five values), have been obtained by means of a standard procedure. Using the values for $J(\omega_N)$ and $J(\omega_H)$ extracted in this manner and the experimental value for $R_1(C_z'N_z[^1H]) - R_1(C_z'N_z[^2D])$, the spectral density of interest, $J(\omega_D + \omega_N)$, was calculated according to eq 2a. (Note that in this approach the determined values of $J(\omega_D + \omega_N)$ are affected by the same uncertainties that influence conventional ^{15}N relaxation analyses—for example, CSA variability and R_{ex}.)

The results for three typical residues are shown in Figure 7 (the choice of residues is described below). The filled diamonds in the plot correspond to the five spectral densities derived by means of the reduced spectral density mapping procedure using the conventional ^{15}N relaxation rates (see above). These five points were fitted using the Lipari−Szabo "model-free" spectral density $J_{LS}(\omega) = (1/5)\{S^2(\tau_c/(1 + \omega^2\tau_c^2)) + (1 - S^2)(\tau_m/(1 + \omega^2\tau_m^2))\}$, where τ_c, S^2, and τ_e are fitting parameters and $\tau_m = 1/(\tau_c^{-1} + \tau_e^{-1})$. The resulting best-fit curves are shown in Figure 7. Shown in the same graph are the new spectral densities $J(\omega_D + \omega_N)$ derived as described above (open circles and squares, corresponding to 500 and 600 MHz data, respectively). Errors indicated in Figure 7 for $J(\omega_D + \omega_N)$ reflect only the uncertainties in the measurement of $R_1(C_z'N_z[^1H/^2D])$ (same as in Figure 6a) and ignore uncertainties associated with the spectral density mapping procedure and subsequent subtraction of the spectral densities.

One of the goals of this work has been to use the extracted values of $J(\omega_D + \omega_N)$ as a "check" of the motional model, i.e., in this case the Lipari−Szabo model. The deviation between experimentally determined values of $J(\omega_D + \omega_N)$ (open symbols in Figure 7) and values predicted using the Lipari−Szabo spectral density (continuous curves in Figure 7) have been calculated according to $\chi_{LS}^2 = \sum_{\{500,600\}}(J(\omega_D + \omega_N) - J_{LS}(\omega_D + \omega_N))^2$. All residues in the protein were subsequently sorted according to the magnitude of χ_{LS}^2, and three residues, Glu-25, Lys-41, and Gly-45, were selected precisely from the middle of the sorted list. These residues, therefore, illustrate the typical level of agreement between the experimentally determined values of $J(\omega_D + \omega_N)$ and the Lipari−Szabo curve.

In general, the newly obtained spectral densities are consistent with Lipari−Szabo profiles that are based on $J(0)$, $J(\omega_N)$, and $J(\omega_H)$, Figure 7. The deviations observed in the graphs appear to be random in character and are largely due to the error propagation in the mapping procedure, as described above. Note that the pair of points at frequencies of 26.1 and 31.3 MHz ($(\omega_D + \omega_N)/2\pi$ evaluated at 500 and 600 MHz) greatly improves the sampling of the spectral density profile in its most informative part. In principle, as a next step, the difference $R_2(C_z'N_x[^1H]) - R_2(C_z'N_x[^2D])$ can be used to extract $J(\omega_D)$, eq 2b. However, because this term is small in comparison to $J(0)$, we anticipate that the error propagation problem will become severe in such calculations. In any event, $J(\omega_D)$ lies in a region of the spectral density curve that is sufficiently well defined by conventional $^{15}N[^1H]$ data measured at multiple fields and is, therefore, less interesting than $J(\omega_D + \omega_N)$.

Conclusion

A $^{15}N[^2D]$ relaxation probe of protein backbone dynamics has been introduced in this work. The new experiments complement the more conventional $^{15}N[^1H]$ measurements and provide access to the spectral density $J(\omega_D + \omega_N)$, which is particularly sensitive to lower-frequency motions.

The combinations $R_1(C_z'N_z[^1H]) - R_1(C_z'N_z[^2D])$ and $R_2(C_z'N_x[^1H]) - R_2(C_z'N_x[^2D])$ derived from the new measurements are "clean" as they depend only on dipolar relaxation

(90) Peng, J. W.; Wagner, G. *Biochemistry* **1995**, *34*, 16733−16752.
(91) Farrow, N. A.; Zhang, O. W.; Forman-Kay, J. D.; Kay, L. E. *Biochemistry* **1995**, *34*, 868−878.
(92) Farrow, N. A.; Zhang, O. W.; Szabo, A.; Torchia, D. A.; Kay, L. E. *J. Biomol. NMR* **1995**, *6*, 153−162.

terms and are free from uncertainties associated with CSA contributions, R_{ex}, and a number of minor relaxation contributions. In this sense, the new experiments may provide an opportunity to measure very accurate absolute values of the order parameters S^2, as long as sensitivity is not limiting. While in most situations it is the *relative* variations of S^2 that are most important (e.g., as a function of residue number or in the context of ligand binding), reliable *absolute* values of S^2 are needed for comparing data obtained from different relaxation probes (^{15}N, ^{13}C, ^{2}D, etc.), for comparing the results of relaxation measurements with molecular dynamics simulations,[93] or for interpreting relaxation data in terms of entropy.[94]

The $^{15}N[^{2}D]$ and $^{15}N[^{1}H]$ relaxation rates measured in protein L are, in general, consistent, as are the dynamic parameters extracted from both sets of data. In addition, $J(\omega_D + \omega_N)$ values obtained from these measurements agree with predictions based on the Lipari−Szabo interpretation of conventional ^{15}N relaxation data, supporting the use of the Lipari−Szabo model in studies of backbone dynamics. The new methodology presented here will be of particular interest in the study of unfolded and partially unfolded protein states. In these applications R_{ex} can be substantial, complicating the interpretation of conventional ^{15}N transverse relaxation data. In addition, the fact that nanosecond time scale dynamics can be explored more fully through measurement of $J(\omega_D + \omega_N)$ suggests that these new experiments will be particularly useful for studying "dynamic" molecules that display a broad spectrum of motions. We are currently pursuing a number of such applications.

Acknowledgment. We thank Dr. Klaas Hallenga (University of Wisconsin, Madison) and Dr. Ranjith Muhandiram (University of Toronto) for their help and valuable discussions. O.M. acknowledges the support of an EMBO postdoctoral fellowship. L.E.K. holds a Canada Research Chair in Biochemistry.

Supporting Information Available: Figures showing $^{1}H^{\alpha}-^{15}N[^{1}H/^{2}D]$ correlation maps for $R_1(C_z'N_z[^{1}H/^{2}D])$ measurements at 600 MHz, selected $R_1(C_z'N_z[^{1}H/^{2}D])$ and $R_{1\rho}(C_z'N_x[^{1}H/^{2}D])$ relaxation curves, and a summary of relaxation rates in protein L at 500 MHz (PDF). This material is available free of charge via the Internet at http://pubs.acs.org.

JA040215Z

(93) Smith, L. J.; Mark, A. E.; Dobson, C. M.; van Gunsteren, W. F. *Biochemistry* **1995**, *34*, 10918−10931.
(94) Yang, D. W.; Kay, L. E. *J. Mol. Biol.* **1996**, *263*, 369−382.